4304–4316 *Nucleic Acids Research, 2016, Vol. 44, No. 9* *Published online 15 April 2016*
doi: 10.1093/nar/gkw244

Ribosome biogenesis factor Tsr3 is the aminocarboxypropyl transferase responsible for 18S rRNA hypermodification in yeast and humans

Britta Meyer[1,†], Jan Philip Wurm[1,2,†], Sunny Sharma[3], Carina Immer[1,2], Denys Pogoryelov[4], Peter Kötter[1], Denis L. J. Lafontaine[3], Jens Wöhnert[1,2,*] and Karl-Dieter Entian[1,*]

[1]Institute for Molecular Biosciences, Goethe University, Frankfurt/M, Germany, [2]Center of Biomolecular Magnetic Resonance, Goethe University, Frankfurt/M, Germany, [3]RNA Molecular Biology & Center for Microscopy and Molecular Imaging, Fonds National de la Recherche Scientifique (F.R.S./FNRS), Université Libre de Bruxelles (ULB) and [4]Institute of Biochemistry, Goethe University, Frankfurt/M, Germany

Received February 04, 2016; Revised March 24, 2016; Accepted March 28, 2016

ABSTRACT

The chemically most complex modification in eukaryotic rRNA is the conserved hypermodified nucleotide N1-methyl-N3-aminocarboxypropyl-pseudouridine ($m^1acp^3\Psi$) located next to the P-site tRNA on the small subunit 18S rRNA. While S-adenosylmethionine was identified as the source of the aminocarboxypropyl (acp) group more than 40 years ago the enzyme catalyzing the acp transfer remained elusive. Here we identify the cytoplasmic ribosome biogenesis protein Tsr3 as the responsible enzyme in yeast and human cells. In functionally impaired Tsr3-mutants, a reduced level of acp modification directly correlates with increased 20S pre-rRNA accumulation. The crystal structure of archaeal Tsr3 homologs revealed the same fold as in SPOUT-class RNA-methyltransferases but a distinct SAM binding mode. This unique SAM binding mode explains why Tsr3 transfers the acp and not the methyl group of SAM to its substrate. Structurally, Tsr3 therefore represents a novel class of acp transferase enzymes.

INTRODUCTION

Eukaryotic ribosome biogenesis is highly complex and requires a large number of non-ribosomal proteins and small non-coding RNAs in addition to ribosomal RNAs (rRNAs) and proteins (1). An increasing number of diseases—so called ribosomopathies—are associated with disturbed ribosome biogenesis (2–4).

During eukaryotic ribosome biogenesis several dozens of rRNA nucleotides become chemically modified (1). The most abundant rRNA modifications are methylations at the 2′-OH ribose moieties and isomerizations of uridine residues to pseudouridine, catalyzed by small nucleolar ribonucleoprotein particles (snoRNPs) (5,6). In addition, 18S and 25S (yeast)/ 28S (humans) rRNAs contain several base modifications catalyzed by site-specific and snoRNA-independent enzymes. In *Saccharomyces cerevisiae* 18S rRNA contains four base methylations, two acetylations and a single 3-amino-3-carboxypropyl (acp) modification, whereas six base methylations are present in the 25S rRNA (7). While in humans the 18S rRNA base modifications are highly conserved, only three of the yeast base modifications catalyzed by *Sc*Rrp8/*Hs*NML (8), *Sc*Rcm1/*Hs*NSUN5 and *Sc*Nop2/*Hs*NSUN1 (9,10) are preserved in the corresponding human 28S rRNA.

Ribosomal RNA modifications have been suggested to optimize ribosome function, although in most cases this remains to be clearly established. They might contribute to increased RNA stability by providing additional hydrogen bonds (pseudouridines), improved base stacking (pseudouridines and base methylations) or an increased resistance against hydrolysis (ribose methylations) (11–13). Most modified rRNA nucleotides cluster in the vicinity of the decoding or the peptidyl transferase center, suggesting an influence on ribosome functionality and stability (14–16). Defects of rRNA modification enzymes often lead to disturbed ribosome biogenesis or functionally impaired ribosomes, although the lack of individual rRNA modifications often has no or only a slight influence on the cell (16,17). Importantly, malfunctions of several base modifying enzymes are linked to developmental diseases (18,2,19), aging (10) or tumorigenesis (20).

The chemically most complex modification is located in the loop capping helix 31 of 18S rRNA (Supplementary Figure S1B). There a uridine (U1191 in yeast) is modified

*To whom correspondence should be addressed. Tel: +49 69 79829525; Fax: +49 69 79829527; Email: entian@bio.uni-frankfurt.de
Correspondence may also be addressed to Jens Wöhnert. Tel: +49 69 79829785; Fax: +49 69 79829527; Email: woehnert@bio.uni-frankfurt.de
† These authors contributed equally to the paper as first authors.

to 1-methyl-3-(3-amino-3-carboxypropyl)-pseudouridine ($m^1acp^3\Psi$, Figure 1A). This base modification was first described in 1968 for hamster cells (21) and is conserved in eukaryotes. This hypermodified nucleotide, which is located at the P-site tRNA, is synthesized in three steps beginning with the snR35 H/ACA snoRNP guided conversion of uridine into pseudouridine (22). In a second step, the essential SPOUT-class methyltransferase Nep1/Emg1 modifies the pseudouridine to N1-methylpseudouridine (23–25). Methylation can only occur once pseudouridylation has taken place, as the latter reaction generates the substrate for the former. The final acp modification leading to N1-methyl-N3-aminocarboxypropyl-pseudouridine occurs late during 40S biogenesis in the cytoplasm (26,27), while the two former reactions are taking place in the nucleolus and nucleus, and is independent from pseudouridylation or methylation (25). Both the methyl and the acp group are derived from S-adenosylmethionine (SAM) (21), but the enzyme responsible for acp modification remained elusive for more than 40 years.

Only a few acp transferring enzymes have been characterized until now (28). During the biosynthesis of wybutosine, a tricyclic nucleoside present in eukaryotic and archaeal phenylalanine tRNA (29), Tyw2 (Trm12 in yeast) transfers an acp group from SAM to an acidic carbon atom. Archaeal Tyw2 has a structure very similar to Rossmann-fold (class I) RNA-methyltransferases (30), but its distinctive SAM-binding mode enables the transfer of the acp group instead of the methyl group of the cofactor. Another acp modification has been described in the diphtamide biosynthesis pathway (31), where an acp group is transferred from SAM to the carbon atom of a histidine residue of eukaryotic translation elongation factor 2 by use of a radical mechanism (32,33).

In a recent bioinformatic study, the uncharacterized yeast gene *YOR006c* was predicted to be involved in ribosome biogenesis (34). It is highly conserved among eukaryotes and archaea (Supplementary Figure S1A) and its deletion leads to an accumulation of the 20S pre-rRNA precursor of 18S rRNA, suggesting an influence on D-site cleavage during the maturation of the small ribosomal subunit. On this basis, *YOR006C* was renamed 'Twenty S rRNA accumulation 3′ (*TSR3*). However, its function remained unclear although recently a putative nuclease function during 18S rRNA maturation was predicted (35).

Here, we identify Tsr3 as the long-sought acp transferase that catalyzes the last step in the biosynthesis of the hypermodified nucleotide $m^1acp^3\Psi$ in yeast and human cells. Furthermore using catalytically defective mutants of yeast Tsr3 we demonstrated that the acp modification is required for 18S rRNA maturation. Surprisingly, the crystal structures of archaeal homologs revealed that Tsr3 is structurally similar to the SPOUT-class RNA methyltransferases. In contrast, the only other structurally characterized acp transferase enzyme Tyw2 belongs to the Rossmann-fold class of methyltransferase proteins. Interestingly, the two structurally very different enzymes use similar strategies in binding the SAM-cofactor in order to ensure that in contrast to methyltransferases the acp and not the methyl group of SAM is transferred to the substrate.

MATERIALS AND METHODS

Genetic constructions, growth conditions and yeast media

Detailed descriptions are available in Supplementary Data.

Cell culture

HCT116(+/+) cells (CCL-247; ATCC) were grown at 37°C in a humidified incubator under 5% CO_2 in the McCoy's 5a modified (Sigma-Aldrich)/10% FBS media. All media were supplemented with 50 U/ml penicillin and 50 μg/ml streptomycin (Life Technologies).

DsiRNA inactivation and RT-qPCR

Reverse transfection of HCT116 cells, DsiRNA inactivation and RT-qPCR using total human RNA are described in Supplementary Data.

Sucrose gradient analysis

Detailed descriptions for analytical or preparative separations of ribosomal subunits or polysome gradients are provided in Supplementary Data.

HPLC analysis of 18S rRNA nucleosides

40S subunits from 200 ml yeast culture were isolated by sucrose gradient centrifugation in a SW28 rotor as described above, and precipitated with 2.5 vol of 100% ethanol (−20°C over night). Precipitated 40S subunits were dissolved in water and the 18S rRNA was purified via spin columns (Ambion PureLink RNA Mini Kit). RNA fragments were hydrolysed and dephosphorylated as described by Gehrke and Kuo (36). HPLC analysis of rRNA nucleoside composition was performed using a Supelcosil LC-18S column (Sigma; 250 × 4.6 mm, 5 μm) with a pre-column (4.6 × 20 mm) as previously described (25).

^{14}C labeling of 18S rRNA nucleotide Ψ(U)1191

To enhance ^{14}C-labeling, mutants of interest were recombined with a *Δmet13* deletion. Resulting strains were cultivated with L-[1-^{14}C]-methionine (Hartmann Analytic, 0.1 mCi/ml, 54 mCi/mmol) as described before (25). From isotope labeled cells total RNA was isolated with the PureLink RNA Mini Kit (Ambion) after enzymatic cell lysis with zymolyase. Ribosomal RNAs were separated on a 4% denaturing polyacrylamide gel. After ethidium bromide straining gels were dried and analyzed by autoradiography for 3–5 days using a storage phosphor screen. Signals were visualized with the Typhoon 9100 (GE Healthcare).

Northern blot analysis

5 μg of total yeast RNAs extracted with phenol/chloroform were separated on 1.2% agarose gels in BPTE buffer for 16 h at 60V (37) and afterwards transferred to a Biodyne B membrane by vacuum blotting. Oligonucleotides D/A2 or +1-A0 were radiolabeled using γ-[^{32}P]-ATP and T4-polynucleotide kinase and hybridized to the membrane at

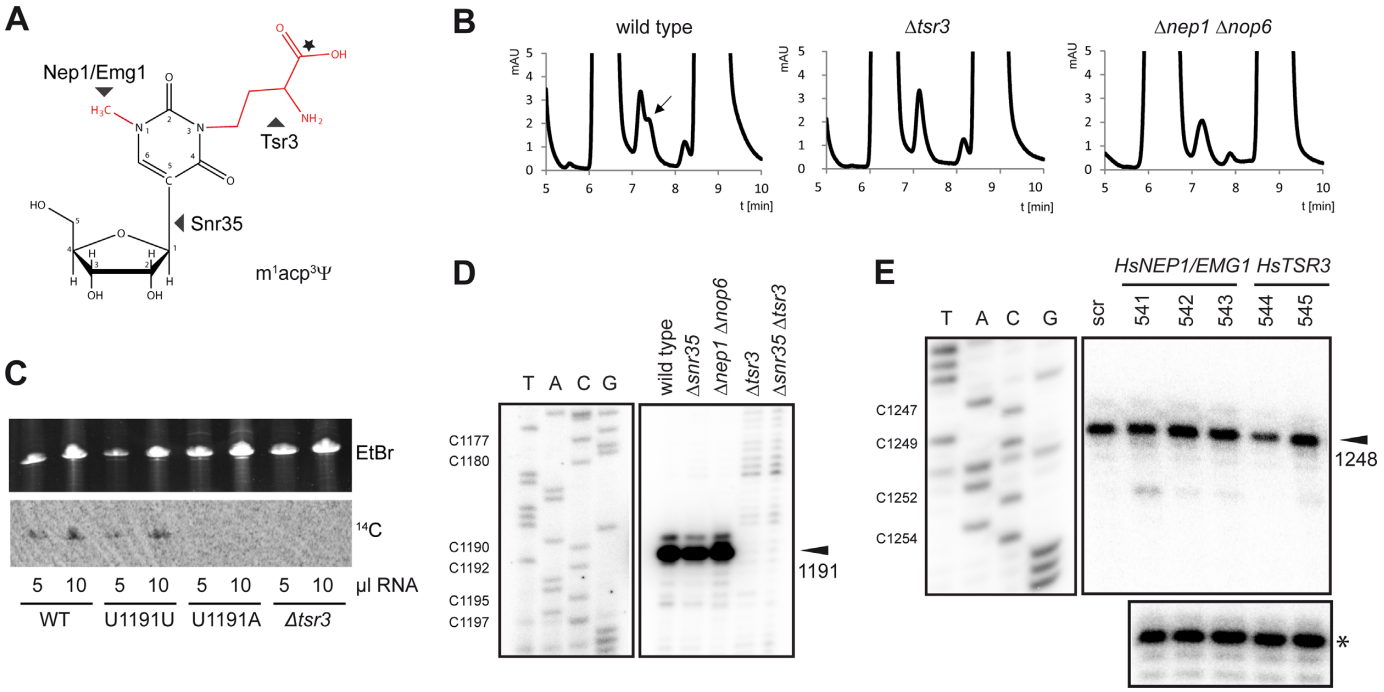

Figure 1. Tsr3 is necessary for acp modification of 18S rRNA in yeast and human. (**A**) Hypermodified nucleotide $m^1acp^3\Psi$ is synthesized in three steps: pseudouridylation catalyzed by snoRNP35, N1-methylation catalyzed by methyltransferase Nep1 and N3-acp modification catalyzed by Tsr3. The asterisk indicates the C1-atom labeled in the ^{14}C-incorporation assay. (**B**) RP-HPLC elution profile of yeast 18S rRNA nucleosides. Hypermodified $m^1acp^3\Psi$ elutes at 7.4 min (wild type, left profile) and is missing in *Δtsr3* (middle profile) and *Δnep1 Δnop6* mutants (right profile). (**C**) ^{14}C-acp labeling of 18S rRNAs. Wild type (WT) and plasmid encoded 18S rRNA (U1191U) show the ^{14}C-acp signal, whereas the ^{14}C-acp signal is missing in the U1191A mutant plasmid encoded 18S rRNA (U1191A) and *Δtsr3* mutants (*Δtsr3*). Upper lanes show the ethidium bromide staining of the 18S rRNAs for quantification. All samples were loaded on the gel with two different amounts of 5 and 10 µl. (**D**) Primer extension analysis of acp modification in yeast 18S rRNA (right gel) including a sequencing ladder (left gel). The primer extension stop at nucleotide 1191 is missing exclusively in *Δtsr3* mutants and *Δtsr3 Δsnr35* recombinants. (**E**) Primer extension analysis of human 18S rRNA after siRNA knockdown of *HsNEP1/EMG1* (541, 542 and 543) and *HsTSR3* (544 and 545) (right gel), including a sequencing ladder (left gel). The primer extension arrest is reduced in HTC116 cells transfected with siRNAs 544 and 545. The efficiency of siRNA mediated *HsTSR3* repression correlates with the primer extension signals (see Supplementary Figure S2A). As a loading control, a structural stop is shown (asterisks).

37°C. Signals were visualized by phosphoimaging with the Typhoon 9100 (GE Healthcare). RNA extraction from human cells, gel-electrophoresis and northern blotting were performed as described before (38).

Primer extension

20 pmol of oligonucleotide PE-1191 complementary to yeast 18S rRNA nucleotides 1247–1228 were labeled with 50 µCi γ-[^{32}P]-ATP using T4-polynucleotide kinase, purified via Sephadex G-25 and annealed to 500 ng of 18S rRNA. Primer annealing and reverse transcription were carried out as described by Sharma *et al.* (39). After precipitation with ethanol and 3 M NaAc pH 5.2 pellets were washed with 70% ethanol, dried and dissolved in 12 µl formamide loading dye. 2 µl of primer extension samples were separated on sequencing or mini gels which were dried after running and exposed on a storage phosphor screen. Signals were visualized with the Typhoon 9100 (GE Healthcare).

Primer extension on human RNA was performed using 5 µg of total RNA with AMV Reverse Transcriptase (Promega) and oligonucleotide PE_1248. Following alkaline hydrolysis, cDNAs were precipitated with ethanol, resuspended in acrylamide loading buffer and separated on a 6% (v/v) denaturing acrylamide gel in 0.5× TBE at 80 W for 1.5 h. After migration, the gels were dried and exposed to Fuji Imaging plates (Fujifilm). The signal was acquired with a Phosphor imager (FLA-7000, Fujifilm).

Protein detection and localization

A description of the western blot detection of HA-fused Tsr3 in yeast crude extracts or sucrose gradients fractions is provided in Supplementary Data. For cellular localization Tsr3 was expressed as N-terminal fusion with yEGFP in a yeast strain encoding for *Sc*Nop56-mRFP (40). Protein localization in exponentially growing cells was visualized using a Leica TCS SP5.

In vitro SAM binding

Purified *Ss*Tsr3 protein in 25 mM Tris–HCl pH 7.8 250 mM NaCl was mixed with S-[methyl-^{14}C]-adenosyl-L-methionine (PerkinElmer; 20 µCi/ml, 58 mCi/mmol) and 0–10 mM non-labeled SAM in a binding buffer (50 mM Tris–HCl pH 7.8, 250 mM NaCl) in a total volume of 50 µl and incubated at 30°C for 10 min. Samples were passed over HAWP02500 membrane filters (Millipore) and unbound ^{14}C-SAM was removed by washing three times with 5 ml buffer using a vacuum filtering equipment. Filter bound

^{14}C-SAM was measured by liquid scintillation spectrometry in a Wallac 1401 scintillation counter.

Protein expression and purification

Genes coding for archaeal Tsr3 homologs without any tags were obtained commercially (Genscript) in pET11a vectors and overexpressed in *Escherichia coli* BL21(DE3). Proteins were purified by a combination of heat shock and appropriate column chromatography steps as described in detail in the Supplementary Data.

Crystallization, X-ray data collection, structure calculation and refinement

Initial hits for *Vd*Tsr3 and *Ss*Tsr3 were obtained using the Morpheus Screen (Molecular dimensions) and further refined as described in the Supplementary Data. Diffraction data were collected at the Swiss Light Source (Paul Scherer Institut). The structure of *Vd*Tsr3 was determined at 1.6 Å by SAD using a selenomethionine derivative. The structure of *Ss*Tsr3 was determined at 2.25 Å by molecular replacement using *Vd*Tsr3 as the search model. A detailed description of the data collection, processing, structure calculation and refinement procedures can be found in the Supplementary Data and in Supplementary Table S1. Structures were deposited in the Protein Data Bank as entries 5APG (*Vd*Tsr3) and 5AP8 (*Ss*Tsr3).

Analytical gel filtration

For analytical gel filtration experiments a Sephadex S75 10/300 GL column (GE Healthcare) was used. 100 µl protein samples (25 mM Tris–HCl pH 7.8, 250 mM NaCl, 2 mM β-mercaptoethanol) with a protein concentration of 150 µM were used. The flow rate was 0.5 ml/min. The column was calibrated using the marker proteins of the LMW gel filtration calibration kit (GE Healthcare). Protein elution was followed by recording the adsorption at a wavelength of $\lambda = 280$ nm.

Fluorescence quenching and fluorescence anisotropy measurements

Fluorescence quenching and fluorescence anisotropy measurements were carried out in triplicates at 25°C on a Fluorolog 3 spectrometer (Horiba Jobin Yvon) equipped with polarizers. For fluorescence quenching with SAM, SAH and 5′-methylthioadenosine experiments the tryptophan fluorescence of *Ss*Tsr3 (200 nM in 25 mM Tris–HCl pH 7.8, 250 mM NaCl, 2 mM β-mercaptoethanol) was excited at 295 nm and emission spectra were recorded from 250 to 450 nm for each titration step. The fluorescence intensity at 351 nm for each titration step was normalized with regard to the fluorescence of the free protein and was used for deriving binding curves. K_D's were derived by nonlinear regression with Origin 8.0 (Origin Labs) using Equation (1):

$$F = a \cdot \frac{c}{c + K_D} + 1 \quad (1)$$

(F is the normalized fluorescence intensity, a is the change in fluorescence intensity, c is the ligand concentration and K_D is the dissociation constant).

5′-Fluoresceine labeled RNAs for fluorescence anisotropy measurements were obtained commercially (Dharmacon), deprotected according to the manufacturer's protocol and the RNA concentration adjusted to 50 nM in 25 mM Tris–HCl pH 7.8, 250 mM NaCl. Fluoresceine fluorescence was excited at 492 nm and emission was recorded at 516 nm. The data were fitted to Equation (1) (F is the normalized fluorescence anisotropy, a is the change in fluorescence anisotropy).

RESULTS

Tsr3 is the enzyme responsible for 18S rRNA acp modification in yeast and humans

The *S. cerevisiae* 18S rRNA acp transferase was identified in a systematic genetic screen where numerous deletion mutants from the EUROSCARF strain collection (www.euroscarf.de) were analyzed by HPLC for alterations in 18S rRNA base modifications.

For the *Δtsr3* deletion strain the HPLC elution profile of 18S rRNA nucleosides (Figure 1B) was very similar to that of the pseudouridine-N1 methyltransferase mutant *Δnep1,* where a shoulder at ∼ 7.4 min elution time was missing in the elution profile. As previously reported this shoulder was identified by ESI-MS as corresponding to $m^1acp^3\Psi$ (25). In order to directly analyze the presence of the acp modification of nucleotide 1191 we used an *in vivo* ^{14}C incorporation assay with 1-^{14}C-methionine (25). Whereas the acp labeling of 18S rRNA was clearly present in the wild type strain no radioactive labeling could be observed in a *Δtsr3* strain (Figure 1C). No radioactive labeling was detected in the 18S U1191A mutant which served as a control for the specificity of the ^{14}C-aminocarboxypropyl incorporation.

As previously shown, only the acp but none of the other modifications at U1191 of yeast 18S rRNA blocks reverse transcriptase activity. Therefore the presence of the acp modification can be directly assessed by primer extension (16,27). Indeed, in wild-type yeast a strong primer extension stop signal occurred at position 1192. In contrast, in a *Δtsr3* mutant no primer extension stop signal was present at this position. As expected, in a *Δsnr35* deletion preventing pseudouridylation and N1-methylation (resulting in acp^3U) as well as in a *Δnep1* deletion strain where pseudouridine is not methylated (resulting in $acp^3\Psi$) (25) a primer extension stop signal of similar intensity as in the wild type was observed. In a *Δtsr3 Δsnr35* double deletion strain the 18S rRNA contains an unmodified U and the primer extension stop signal was missing (Figure 1D).

The Tsr3 protein is highly conserved in yeast and humans (50% identity). Human 18S rRNA has also been shown to contain $m^1acp^3\Psi$ in the 18S rRNA at position 1248 (41). After siRNA-mediated depletion of Tsr3 in human colon carcinoma HCT116(+/+) cells the acp primer extension arrest was reduced in comparison to cells transfected with a non-targeting scramble siRNA control (Figure 1E, compare lanes 544 and scramble). The efficiency of siRNA-mediated depletion was established by RT-qPCR and found to be very high with siRNA 544 (Supplementary Figure

S2A, remaining TSR3 mRNA level of 2%). By comparison, treating cells with siRNA 545, which only reduced the TSR3 mRNA to 20%, did not markedly reduced the acp signal. This suggests that low residual levels of *Hs*Tsr3 are sufficient to modify the RNA. As a control for loading, a structural stop is shown (asterisk, Figure 1E). Thus, *Hs*Tsr3 is also responsible for the acp modification of 18S rRNA nucleotide Ψ1248 in helix 31. Similar to yeast, siRNA-mediated depletion of the Ψ1248 N1-methyltransferase Nep1/Emg1 had no influence on the primer extension arrest (Figure 1E).

Phenotypic characterization of *Δtsr3* mutants

Although the acp modification of 18S rRNA is highly conserved in eukaryotes, yeast *Δtsr3* mutants showed only a minor growth defect. However, the *Δtsr3* deletion was synthetic sick with a *Δsnr35* deletion preventing pseudouridylation and Nep1-catalyzed methylation of nucleotide 1191 (Figure 2A). Interestingly, no increased growth defect could be observed for *Δtsr3 Δnep1* recombinants containing the *nep1* suppressor mutation *Δnop6* (42) as well as for *Δtsr3 Δsnr35 Δnep1* recombinants with unmodified U1191 (Supplementary Figure S2D and E).

The influence of the acp modification of nucleotide 1191 on ribosome function was analyzed by treating *Δtsr3* mutants with protein synthesis inhibitors. Similar to a temperature-sensitive *nep1* mutant (43), the *Δtsr3* deletion caused hypersensitivity to paromomycin and, to a lesser extent, to hygromycin B (Figure 2B), but not to G418 or cycloheximide (data not shown). In accordance with the synthetic sick growth phenotype the paromomycin and hygromycin B hypersensitivity further increased in a *Δtsr3 Δsnr35* recombination strain (Figure 2B).

In a yeast *Δtsr3* strain as well as in the *Δtsr3 Δsnr35* recombinant 20S pre-rRNA accumulated significantly and the level of mature 18S rRNA was reduced (Supplementary Figures S2C and S3D), as reported previously (34). A minor effect on 20S rRNA accumulation was also observed for *Δsnr35*, but - probably due to different strain backgrounds – to a weaker extent than described earlier (16). In human cells, the depletion of *Hs*Tsr3 in HCT116(+/+) cells caused an accumulation of the human 20S pre-rRNA equivalent 18S-E suggesting an evolutionary conserved role of Tsr3 in the late steps of 18S rRNA processing (Figure 2C and Supplementary Figure S2B). Surprisingly, early nucleolar processing reactions were also inhibited, and this was observed in both yeast *Δtsr3* cells (see accumulation of 35S in Supplementary Figure S2C) and Tsr3 depleted human cells (see 47S/45S accumulation in Figure 2C and Northern blot quantification in Supplementary Figure S2B).

Consistent with its role in late 18S rRNA processing, *TSR3* deletion leads to a ribosomal subunit imbalance with a reduced 40S to 60S ratio of 0.81 ($\sigma = 0.024$) which was further increased in a *Δtsr3 Δsnr35* recombinant to 0.73 ($\sigma = 0.023$) (Supplementary Figure S2F). In polysome profiles, a reduced level of 80S ribosomes and a strong signal for free 60S subunits was observed in line with the 40S subunit deficiency (Supplementary Figure S2G).

Cellular localization of Tsr3 in *S. cerevisiae*

Fluorescence microscopy of GFP-tagged Tsr3 localized the fusion protein in the cytoplasm of yeast cells and no co-localization with the nucleolar marker protein Nop56 could be observed (Figure 2D). This agrees with previous biochemical data suggesting that the acp modification of 18S rRNA occurs late during 40S subunit biogenesis in the cytoplasm (26,27), and makes an additional nuclear localization as reported in a previous large-scale analysis (40) unlikely. After polysome gradient separation C-terminally epitope-labeled Tsr3-3xHA was exclusively detectable in the low-density fraction (Figure 2E). Such distribution on a density gradient suggests that Tsr3 only interacts transiently with pre-40S subunits, which presumably explains why it was not characterized in pre-ribosome affinity purifications.

Structure of Tsr3

Searches for sequence homologs of *S. cerevisiae* Tsr3 (*Sc*Tsr3) by us and others (44) revealed that the genomes of many archaea contain genes encoding Tsr3-like proteins. However, these archaeal homologs are significantly smaller than *Sc*Tsr3 (~190 aa in archaea vs. 313 aa in yeast) due to shortened N- and C-termini (Supplementary Figure S1A).

To locate the domains most important for Tsr3 activity, *Sc*Tsr3 fragments of different lengths containing the highly conserved central part were expressed in a *Δtsr3* mutant (Figure 3A) and analyzed by primer extension (Figure 3B) and Northern blotting (Figure 3C). N-terminal truncations of up to 45 aa and C-terminal truncations of up to 76 aa mediated acp modification as efficiently as the full-length protein and no significant increased levels of 20S pre-RNA were detected. Even a Tsr3 fragment with a 90 aa C-terminal truncation showed a residual primer extension stop, whereas N-terminal truncations exceeding 46 aa almost completely abolished the primer extension arrest (Figure 3B).

Thus, the archaeal homologs correspond to the functional core of Tsr3. In order to define the structural basis for Tsr3 function, homologs from thermophilic archaea were screened for crystallization. We focused on archaeal species containing a putative Nep1 homolog suggesting that these species are in principle capable of synthesizing N1-methyl-N3-acp-pseudouridine. Well diffracting crystals were obtained for Tsr3 homologs from the two crenarchaeal species *Vulcanisaeta distributa* (*Vd*Tsr3) and *Sulfolobus solfataricus* (*Ss*Tsr3) which share 36% (*Vd*Tsr3) and 38% (*Ss*Tsr3) identity with the *Sc*Tsr3 core region (*Sc*Tsr3 aa 46–223). While for *S. solfataricus* the existence of a modified nucleotide of unknown chemical composition in the loop capping helix 31 of its 16S rRNA has been demonstrated (45), no information regarding rRNA modifications is yet available for *V. distributa*.

Crystals of *Vd*Tsr3 diffracted to a resolution of 1.6 Å whereas crystals of *Ss*Tsr3 diffracted to 2.25 Å. Serendipitously, *Vd*Tsr3 was purified and crystallized in complex with endogenous (*E. coli*) SAM (Supplementary Figure S4) while *Ss*Tsr3 crystals contained the protein in the apo state. The structure of *Vd*Tsr3 was solved *ab initio,* by single-wavelength anomalous diffraction phasing (Se-SAD) with

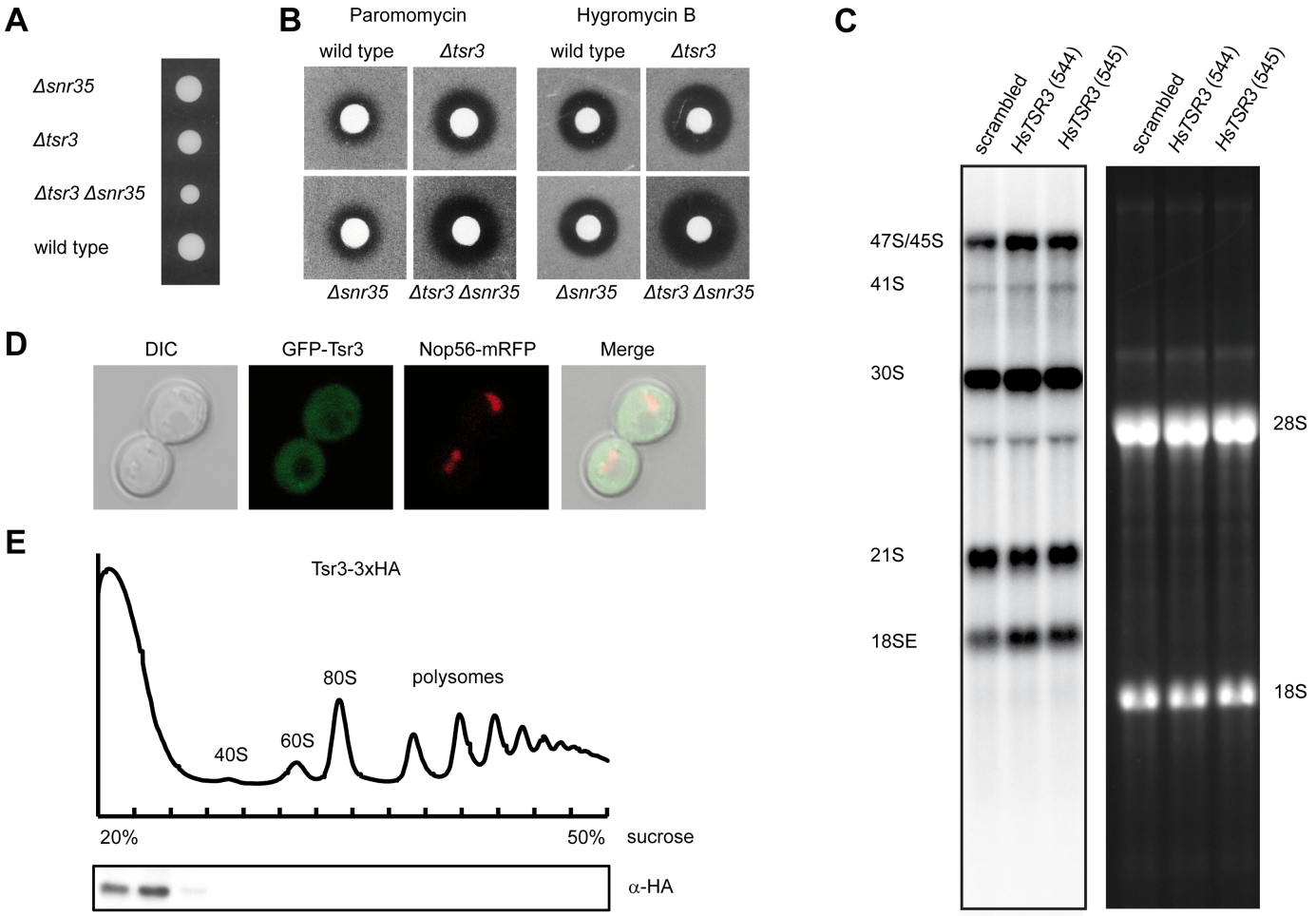

Figure 2. Phenotypic characterization of yeast *TSR3* deletion (*Δtrs*3) and human *TSR3* depletion (siRNAs 544 and 545) and cellular localization of yeast Tsr3. (**A**) Growth of yeast wild type, *Δtsr3*, *Δsnr35 and Δtsr3 Δsnr35* segregants after meiosis and tetrad dissection of *Δtsr3/TSR3 Δsnr35/SNR35* heterozygous diploids. The *Δtsr3* deletion is synthetic sick with a *Δsnr35* deletion preventing U1191 pseudouridylation. (**B**) In agar diffusion assays the yeast *Δtsr3* deletion mutant shows a hypersensitivity against paromomycin and hygromycin B which is further increased by recombination with *Δsnr35*. (**C**) Northern blot analysis with an ITS1 hybridization probe after siRNA depletion of *HsTSR3* (siRNAs 544 and 545) and a scrambled siRNA as control. The accumulation of 18SE and 47S and/or 45S pre-RNAs is enforced upon *HsTSR3* depletion. Right gel: Ethidium bromide staining showing 18S and 28S rRNAs. (**D**) Cytoplasmic localization of yeast Tsr3 shown by fluorescence microscopy of GFP-fused Tsr3. From left to right: differential interference contrast (DIC), green fluorescence of GFP-Tsr3, red fluorescence of Nop56-mRFP as nucleolar marker, and merge of GFP-Tsr3/Nop56-mRFP with DIC. (**E**) Elution profile (A_{254}) after sucrose gradient separation of yeast ribosomal subunits and polysomes (upper part) and western blot analysis of 3xHA tagged Tsr3 (Tsr3-3xHA) after SDS-PAGE separation of polysome profile fractions taken every 20 s (lower part). The *TSR3* gene was genetically modified at its native locus, resulting in a C-terminal fusion of Tsr3 with a 3xHA epitope expressed by the native promotor in yeast strain CEN.BM258-5B.

Se containing derivatives (selenomethionine and seleno-substituted SAM). The structure of *Ss*Tsr3 was solved by molecular replacement using *Vd*Tsr3 as a search model (see Supplementary Table S1 for data collection and refinement statistics). The structure of *Vd*Tsr3 can be divided into two domains (Figure 4A). The N-terminal domain (aa 1–92) has a mixed α/β-structure centered around a five-stranded all-parallel β-sheet (Figure 4B) with the strand order β5↑-β3↑-β4↑-β1↑-β2↑. The loops connecting β1 and β2, β3 and β4 and β4 and β5 include α-helices α1, α2 and α3, respectively. The loop connecting β2 and β3 contains a single turn of a 3_{10}-helix. Helices α1 and α2 are located on one side of the five-stranded β-sheet while α3 packs against the opposite β-sheet surface. The C-terminal domain (aa 93–184) has a globular all α-helical structure comprising α-helices α4 to α9. Both domains are tightly packed against each other. Remarkably, the entire C-terminal domain (92 aa) of the protein is threaded through the loop which connects β-strand β3 and α-helix α2 of the N-terminal domain. Thus, the *Vd*Tsr3 structure contains a deep trefoil knot. The structure of *Ss*Tsr3 in the apo state is very similar to that of *Vd*Tsr3 (Figure 4C) with an RMSD for equivalent Cα atoms of 1.1 Å. The only significant difference in the global structure of the two proteins is the presence of an extended α-helix α8 and the absence of α-helix α9 in *Ss*Tsr3.

Structure predictions suggested that Tsr3 might contain a so-called RLI domain which contains a 'bacterial like' ferredoxin fold and binds two iron-sulfur clusters through eight conserved cysteine residues (46). However, no structural similarity to an RLI-domain was detectable. This is in accordance with the functional analysis of alanine replace-

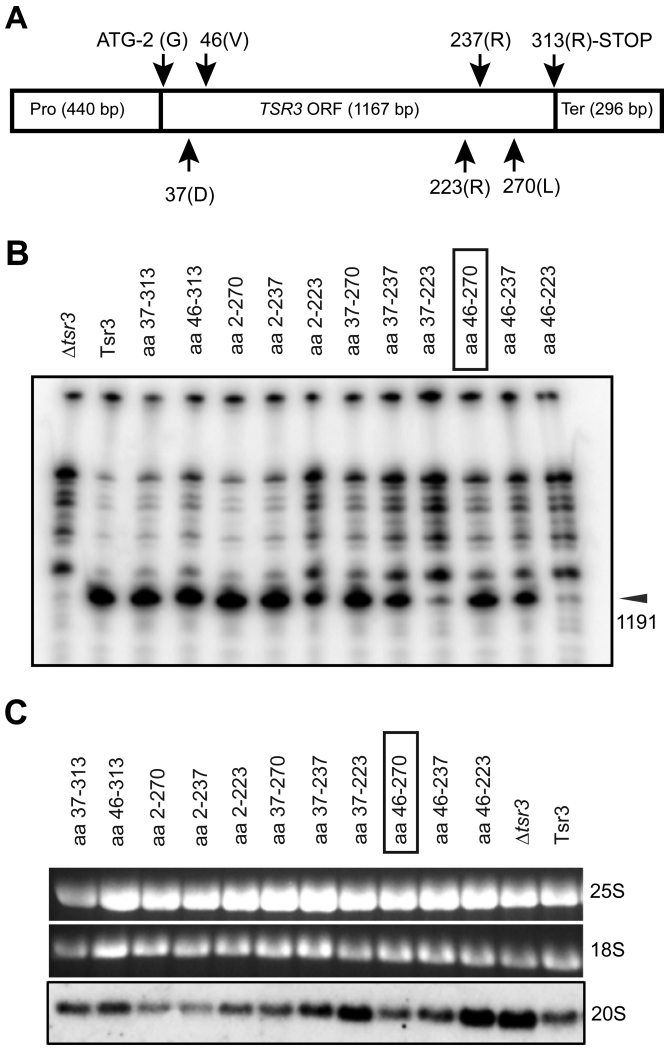

Figure 3. Domain characterization of yeast Tsr3 and correlation of acp modification with late 18S rRNA processing steps. (**A**) Scheme of the *TSR3* gene with truncation positions in the open reading frame. *TSR3* fragments of different length were expressed under the native promotor from multicopy plasmids in a *Δtsr3* deletion strain. (**B**) Primer extension analysis of 18S rRNA acp modification in yeast cells expressing the indicated *TSR3* fragments. N-terminal deletions of 36 or 45 amino acids and C-terminal deletions of 43 or 76 residues show a primer extension stop comparable to the wild type. Tsr3 fragments 37–223 or 46–223 cause a nearly complete loss of the arrest signal. The box highlights the shortest Tsr3 fragment (aa 46–270) with wild type activity (strong primer extension block). (**C**) Northern blot analysis of 20S pre-rRNA accumulation. A weak 20S rRNA signal, indicating normal processing, is observed for Tsr3 fragment 46–270 (highlighted in a box) showing its functionality. Strong 20S rRNA accumulation similar to that of the *Δtsr3* deletion is observed for Tsr3 fragments 37–223 or 46–223.

ment mutations of cysteine residues in *Sc*Tsr3 (Supplementary Figure S3).

The β-strand topology and the deep C-terminal trefoil knot of archaeal Tsr3 are the structural hallmarks of the SPOUT-class RNA-methyltransferase fold. The closest structural homolog identified in a DALI search is the tRNA methyltransferase Trm10 (DALI Z-score 6.8) which methylates the N1 nitrogen of G9/A9 in many archaeal and eukaryotic tRNAs by using SAM as the methyl group donor (47,48). In comparison to Tsr3 the central β-sheet element of Trm10 is extended by one additional β-strand pairing to β2. Furthermore, the trefoil knot of Trm10 is not as deep as that of Tsr3 (Figure 4D). Interestingly, Nep1—the enzyme preceding Tsr3 in the biosynthetic pathway for the synthesis of $m^1acp^3\Psi$—also belongs to the SPOUT-class of RNA methyltransferases. However, the structural similarities between Nep1 and Tsr3 (DALI *Z*-score 4.4) are less pronounced than between Tsr3 and Trm10. Most SPOUT-class RNA-methyltransferases are homodimers. A notable exception is Trm10. Gel filtration experiments with both *Vd*Tsr3 and *Ss*Tsr3 (Figure 4E) showed that both proteins are monomeric in solution thereby extending the structural similarities to Trm10.

So far, structural information is only available for one other enzyme that transfers the acp group from SAM to an RNA nucleotide. This enzyme, Tyw2, is part of the biosynthesis pathway of wybutosine nucleotides in tRNAs. However, there are no structural similarities between Tsr3 and Tyw2, which contains an all-parallel β-sheet of a different topology and no knot structure (30). Instead, Tyw2 has a fold typical for the class-I-or Rossmann-fold class of methyltransferases (Supplementary Figure S5B).

Cofactor binding of Tsr3

The SAM-binding site of Tsr3 is located in a deep crevice between the N- and C-terminal domains in the vicinity of the trefoil knot as typical for SPOUT-class RNA-methyltransferases (Figure 4A). The adenine base of the cofactor is recognized by hydrogen bonds between its N1 nitrogen and the backbone amide of L93 directly preceding β5 as well as between its N6-amino group and the backbone carbonyl group of Y108 located in the loop connecting β5 in the N-terminal and α4 in the C-terminal domain (Figure 5A). Furthermore, the adenine base of SAM is involved in hydrophobic packing interactions with the side chains of L45 (β3), P47 and W73 (α3) in the N-terminal domain as well as with L93, L110 (both in the loop connecting β5 and α4) and A115 (α5) in the C-terminal domain. The ribose 2′ and 3′ hydroxyl groups of SAM are hydrogen bonded to the backbone carbonyl group of I69. The acp side chain of SAM is fixed in position by hydrogen bonding of its carboxylate group to the backbone amide and the side chain hydroxyl group of T19 in α1 as well as the backbone amide group of T112 in α4 (C-terminal domain). Most importantly, the methyl group of SAM is buried in a hydrophobic pocket formed by the sidechains of W73 and A76 both located in α3 (Figure 5A and B). W73 is highly conserved in all known Tsr3 proteins, whereas A76 can be replaced by other hydrophobic amino acids. Consequently, the accessibility of this methyl group for a nucleophilic attack is strongly reduced in comparison with RNA-methyltransferases such as Trm10 (Figure 5B, C). In contrast, the acp side chain of SAM is accessible for reactions in the Tsr3-bound state (Figure 5B).

Binding affinities for SAM and its analogs 5′-methylthioadenosin and SAH to *Ss*Tsr3 were measured using tryptophan fluorescence quenching. *Vd*Tsr3 could not be used in these experiments since we could not purify it in a stable SAM-free form. *Ss*Tsr3 bound SAM

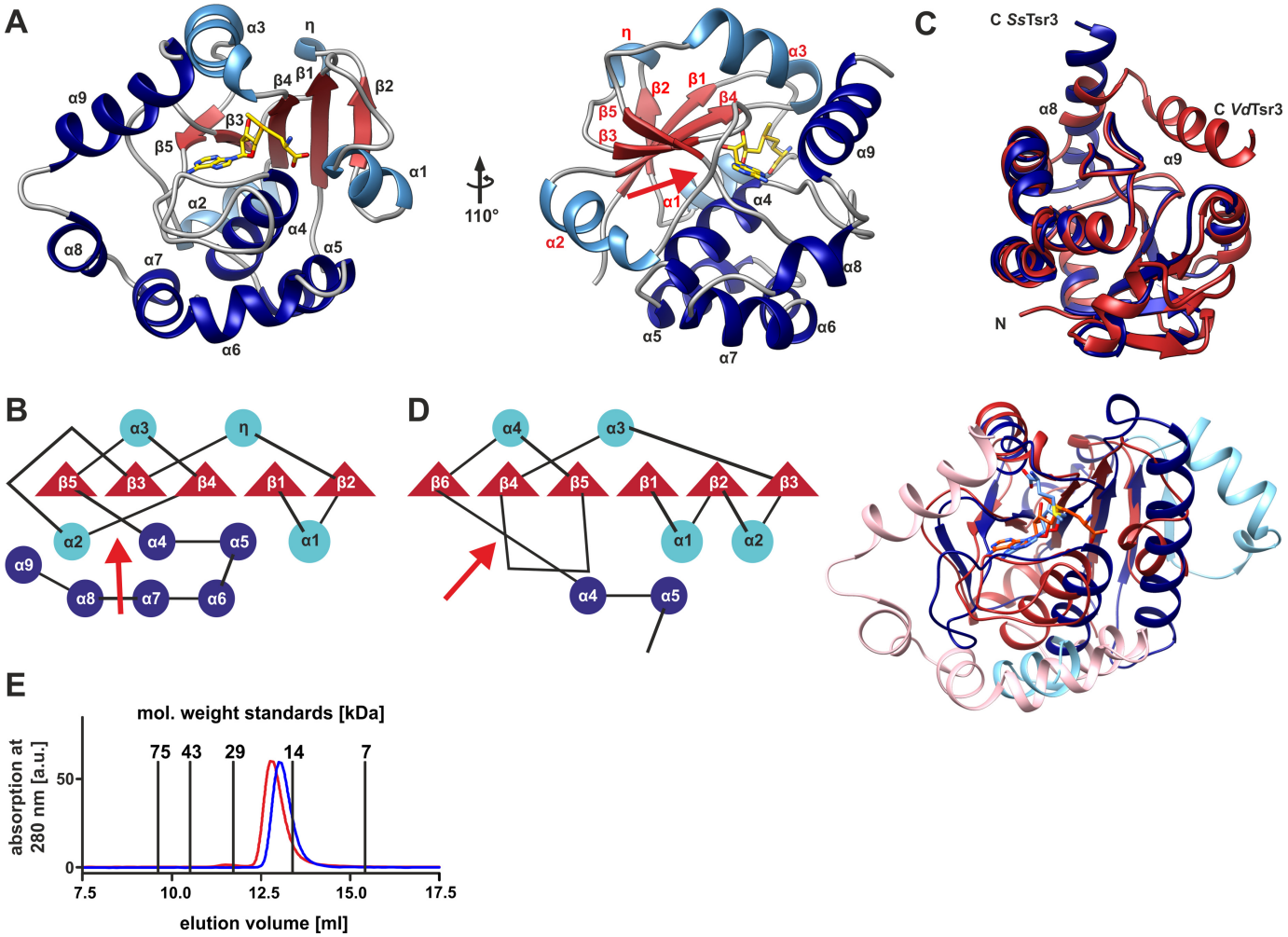

Figure 4. Tsr3 has a fold similar to SPOUT-class RNA methyltransferases. (**A**) Cartoon representation of the X-ray structure of *Vd*Tsr3 in two orientations. β-strands are colored in crimson whereas α-helices in the N-terminal domain are colored light blue and α-helices in the C-terminal domain are colored dark blue. The bound S-adenosylmethionine is shown in a stick representation and colored by atom type. A red arrow marks the location of the topological knot in the structure. (**B**) Secondary structure representation of the *Vd*Tsr3 structure. The color coding is the same as in (A). (**C**) Structural superposition of the X-ray structures of *Vd*Tsr3 in the SAM-bound state (red) and *Ss*Tsr3 (blue) in the apo state. The locations of the α-helix α8 which is longer in *Ss*Tsr3 and of α-helix α9 which is only present in *Vd*Tsr3 are indicated. (**D**) Secondary structure cartoon (left) of *S. pombe* Trm10 (pdb4jwf)—the SPOUT-class RNA methyltransferase structurally most similar to Tsr3 and superposition of the *Vd*Tsr3 and Trm10 X-ray structures (right). (**E**) Analytical gel filtration profiles for *Vd*Tsr3 (red) and *Ss*Tsr3 (blue) show that both proteins are monomeric in solution. Vertical lines indicate the elution volumes of molecular weight markers. *Vd, Vulcanisaeta distributa; Ss, Sulfolobus solfataricus*.

with a K_D of 6.5 μM, which is similar to SAM-K_D's reported for several SPOUT-class methyltransferases. 5′-methylthioadenosin—the reaction product after the acp-transfer—binds only ∼2.5-fold weaker (K_D = 16.7 μM) compared to SAM. S-adenosylhomocysteine which lacks the methyl group of SAM binds with significantly lower affinity (K_D = 55.5 μM) (Figure 5D). This suggests that the hydrophobic interaction between SAM's methyl group and the hydrophobic pocket of Tsr3 is thermodynamically important for the interaction. On the other hand, the loss of hydrogen bonds between the acp sidechain carboxylate group and the protein appears to be thermodynamically less important but these hydrogen bonds might play a crucial role for the proper orientation of the cofactor side chain in the substrate binding pocket.

Accordingly, a W66A-mutation (W73 in *Vd*Tsr3) of *Ss*Tsr3 significantly diminished SAM-binding in a filter binding assay compared to the wild type (Figure 5E). Furthermore, a W to A mutation at the equivalent position W114 in *Sc*Tsr3 strongly reduced the *in vivo* acp transferase activity (Figure 5F). The side chain hydroxyl group of T19 seems of minor importance for SAM binding since mutations of T17 (T19 in *Vd*Tsr3) to either A or D did not significantly influence the SAM-binding affinity of *Ss*Tsr3 (K_D's = 3.9 or 11.2 mM, respectively). Nevertheless, a mutation of the equivalent position S62 of *Sc*Tsr3 to D, but not to A, resulted in reduced acp modification *in vivo*, as shown by primer extension analysis (Figure 5F).

The acp-transfer reaction catalyzed by Tsr3 most likely requires the presence of a catalytic base in order to abstract a proton from the N3 imino group of the modified pseu-

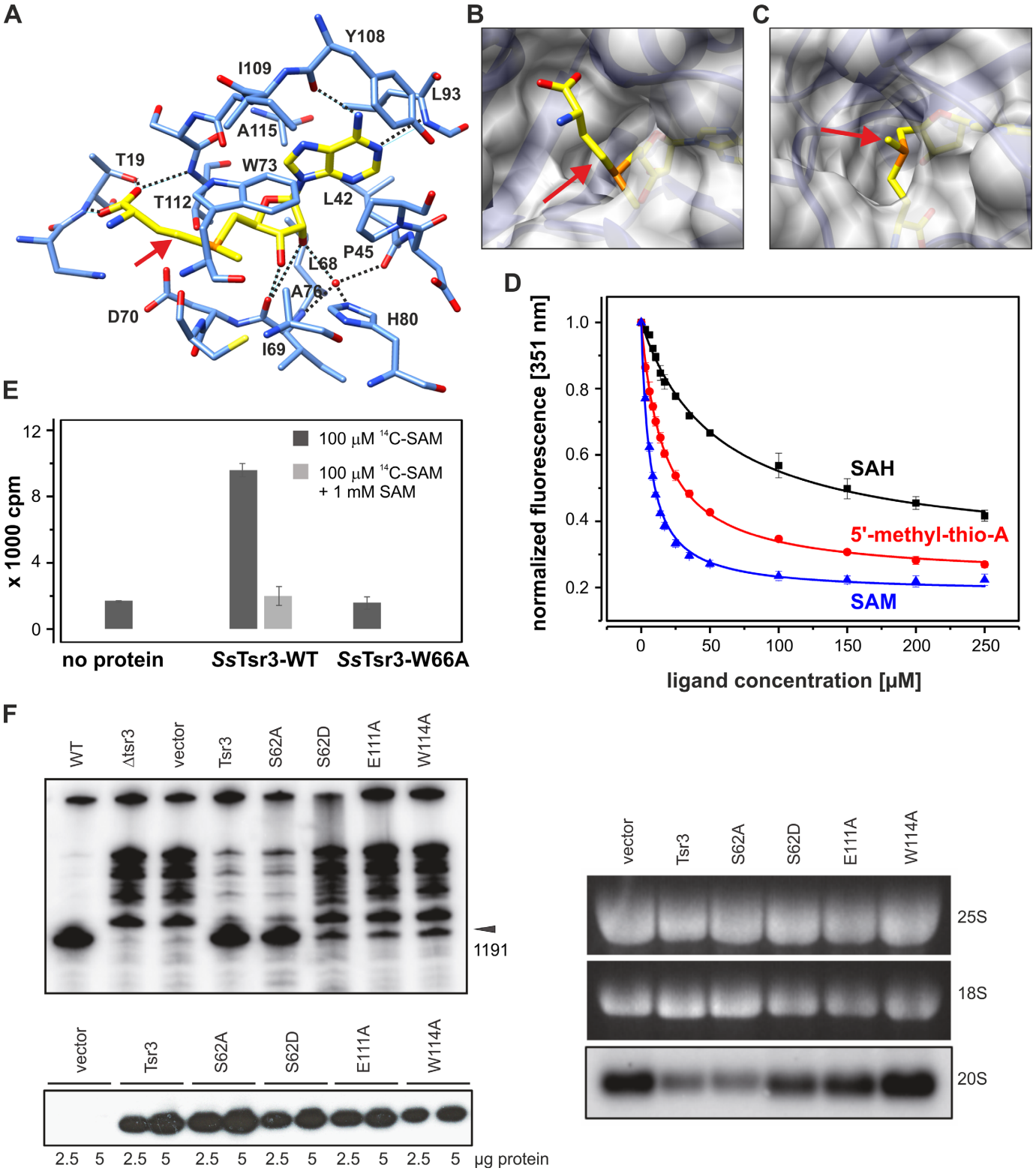

Figure 5. SAM-binding by Tsr3. (**A**) Close-up view of the SAM-binding pocket of *Vd*Tsr3. Nitrogen atoms are dark blue, oxygen atoms red, sulfur atoms orange, carbon atoms of the protein light blue and carbon atoms of SAM yellow. Hydrogen bonds are indicated by dashed lines. (**B**) Solvent accessibility of the acp group of SAM bound to *Vd*Tsr3. The solvent accessible surface of the protein is shown in semitransparent gray whereas SAM is show in a stick representation. Atoms are colored as in (A). A red arrow indicates the reactive CH_2-moiety of the acp group. (**C**) Solvent accessibility of the SAM methyl group for SAM bound to the RNA methyltransferase Trm10. Bound SAM was modelled based on the X-ray structure of the Trm10/SAH-complex (pdb4jwf). A red arrow indicates the SAM methyl group. (**D**) Binding of SAM analogs to *Ss*Tsr3. Tryptophan fluorescence quenching curves upon addition of SAM (blue), 5′-methyl-thioadenosine (red) and SAH (black). (**E**) Binding of ^{14}C-labeled SAM to *Ss*Tsr3. Radioactively labeled SAM is retained on a filter in the presence of *Ss*Tsr3. Addition of unlabeled SAM competes with the binding of labeled SAM. A W66A-mutant of *Ss*Tsr3 (W73 in *Vd*Tsr3) does

douridine. The side chain of D70 (*Vd*Tsr3) located in β4 is ∼5 Å away from the SAM sulfur atom. This residue is conserved as D or E both in archaeal and eukaryotic Tsr3 homologs. Mutations of the corresponding residue in *Ss*Tsr3 to A (D63) does not significantly alter the SAM-binding affinity of the protein ($K_D = 11.0$ μM). However, the mutation of the corresponding residue of *Sc*Tsr3 (E111A) leads to a significant decrease of the acp transferase activity *in vivo* (Figure 5F).

RNA-binding of Tsr3

Analysis of the electrostatic surface properties of *Vd*Tsr3 clearly identified positively charged surface patches in the vicinity of the SAM-binding site suggesting a putative RNA-binding site (Figure 6A). Furthermore, a negatively charged MES-ion is found in the crystal structure of *Vd*Tsr3 complexed to the side chain of K22 in helix α1. Its negatively charged sulfate group might mimic an RNA backbone phosphate. Helix α1 contains two more positively charged amino acids K17 and R25 as does the loop preceding it (R9). A second cluster of positively charged residues is found in or near helix α3 (K74, R75, K82, R85 and K87). Some of these amino acids are conserved between archaeal and eukaryotic Tsr3 (Supplementary Figure S1A). In the C-terminal domain, the surface exposed α-helices α5 and α7 carry a significant amount of positively charged amino acids. A triple mutation of the conserved positively charged residues R60, K65 and R131 to A in *Sc*Tsr3 resulted in a protein with a significantly impaired acp transferase activity *in vivo* (Figure 6D) in line with an important functional role for these positively charged residues.

In order to explore the RNA-ligand specificity of Tsr3 we titrated *Ss*Tsr3 prepared in RNase-free form with 5′-fluoresceine-labeled RNA and determined the affinity by fluorescence anisotropy measurements. *Ss*Tsr3 in the apo state bound a 20mer RNA corresponding to helix 31 of *S. solfataricus* 16S rRNA (Figure 6B) with a K_D of 1.9 μM and to a version of this hairpin stabilized by additional GC base pairs (20mer-GC) with a K_D of 0.6 μM (Figure 6C). A single stranded oligoU-RNA bound with a 10-fold-reduced affinity (6.0 μM). The presence of saturating amounts of SAM (2 mM) did not have a significant influence on the RNA-affinity of *Ss*Tsr3 (K_D of 1.7 μM for the 20mer-GC-RNA) suggesting no cooperativity in substrate binding.

DISCUSSION

U1191 is the only hypermodified base in the yeast 18S rRNA and is strongly conserved in eukaryotes (21,22,26). The formation of 1-methyl-3-(3-amino-3-carboxypropyl)-pseudouridine ($m^1acp^3\Psi$) is very complex requiring three successive modification reactions involving one H/ACA snoRNP (snR35) and two protein enzymes (Nep1/Emg1 and Tsr3). This makes it unique in eukaryotic rRNA modification. The $m^1acp^3\Psi$ base is located at the tip of helix 31 on the 18S rRNA (Supplementary Figure S1B) which, together with helices 18, 24, 34 and 44, contribute to building the decoding center of the small ribosomal subunit (49). A similar modification (acp^3U) was identified in *Haloferax volcanii* (50) and corresponding modified nucleotides were also shown to occur in other archaea (45,51).

As shown here *TSR3* encodes the transferase catalyzing the acp modification as the last step in the biosynthesis of $m^1acp^3\Psi$ in yeast and human cells. Unexpectedly, archaeal Tsr3 has a structure similar to SPOUT-class RNA methyltransferases, and it is the first example for an enzyme of this class transferring an acp group, due to a modified SAM-binding pocket that exposes the acp instead of the methyl group of SAM to its RNA substrate. Similar to the structurally unrelated Rossmann-fold Tyw2 acp transferase, the SAM methyl group of Tsr3 is bound in an inaccessible hydrophobic pocket whereas the acp side chain becomes accessible for a nucleophilic attack by the N3 of pseudouridine. In contrast, in the structurally closely related RNA methyltransferase Trm10 the methyl group of the cofactor SAM is accessible whereas its acp side chain is buried inside the protein. This suggests that enzymes with a SAM-dependent acp transferase activity might have evolved from SAM-dependent methyltransferases by slight modifications of the SAM-binding pocket. Thus, additional examples for acp transferase enzymes might be found with similarities to other structural classes of methyltransferases. In contrast to Nep1 (24), the enzyme preceding Tsr3 in the $m^1acp^3\Psi$ biosynthesis pathway, Tsr3 binds rather weakly and with little specificity to its isolated substrate RNA. This suggests that Tsr3 is not stably incorporated into pre-ribosomal particles and that its binding to the nascent ribosomal subunit possibly requires additional interactions with other pre-ribosomal components. Consistently, in sucrose gradient analysis, Tsr3 was found in low-molecular weight fractions rather than with pre-ribosome containing high-molecular weight fractions.

In contrast to several enzymes that catalyze base specific modifications in rRNAs Tsr3 is not an essential protein. Typically, other small subunit rRNA methyltransferases as Dim1, Bud23 and Nep1/Emg1 carry dual functions, in ribosome biogenesis and rRNA modification, and it is their involvement in pre-RNA processing that is essential rather than their RNA-methylating activity (25,52–55, discussed in 7). In contrast, for several Tsr3 mutants (SAM-binding and cysteine mutations) we found a systematic correlation between the loss of acp modification and the efficiency of 18S rRNA maturation. This demonstrates that, unlike the other small subunit rRNA base modifications, the acp modification is required for efficient pre-rRNA processing.

Recently, structural, functional, and CRAC (cross-linking and cDNA analysis) experiments of late assembly factors involved in cytoplasmic processing of 40S subunits, along with cryo-EM studies of the late pre-40S subunits have provided important insights into late pre-40S processing (56–58). Apart from most of the ribosomal proteins, cy-

←

not bind SAM. (**F**) Primer extension (upper left) shows a strongly reduced acp modification of yeast 18S rRNA in *Δtsr3* cells expressing Tsr3-S62D, -E111A or –W114A. This correlates with a 20S pre-rRNA accumulation comparable to the *Δtsr3* deletion (right: northern blot). 3xHA tagged Tsr3 mutants are expressed comparable to the wild type as shown by western blot (lower left).

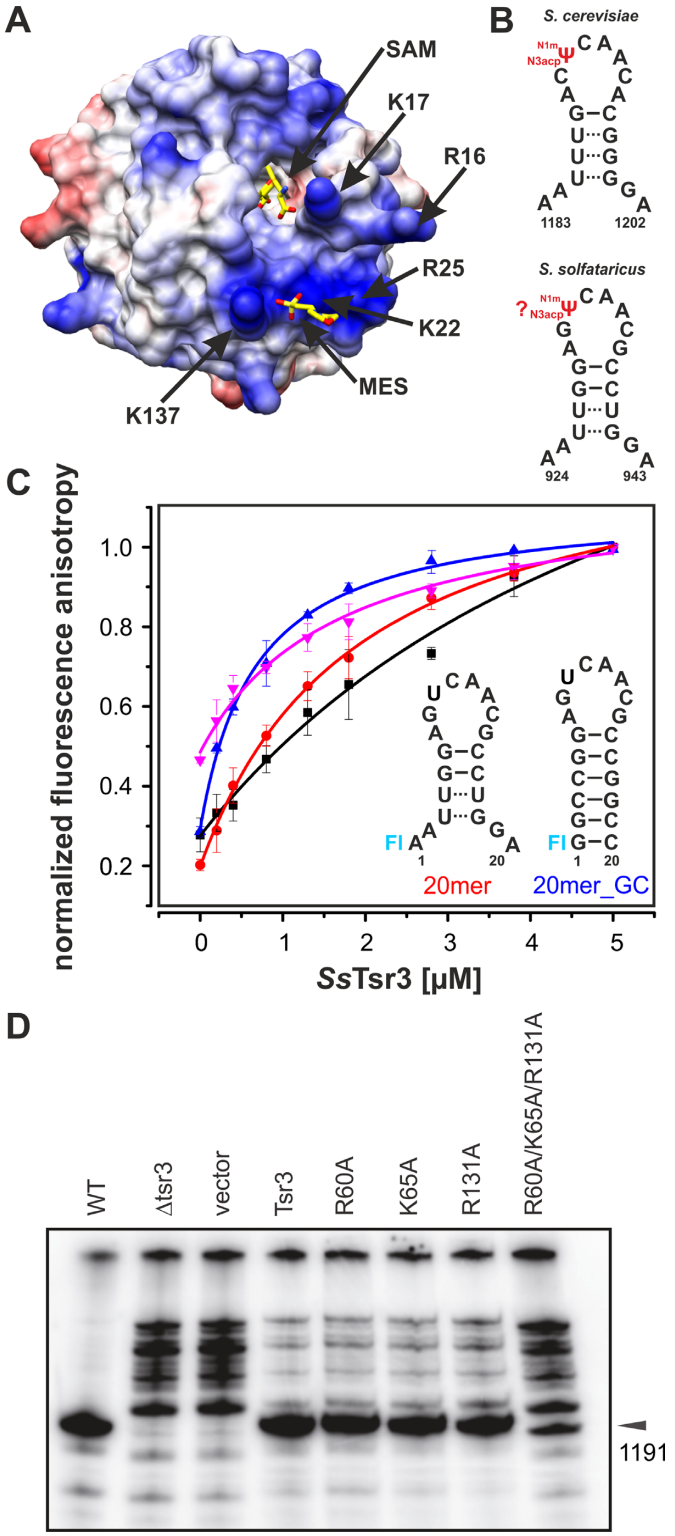

Figure 6. RNA-binding of Tsr3. (**A**) Electrostatic charge distribution on the surface of *Vd*Tsr3. Surface areas colored in blue are positively charged whereas red areas are negatively charged. SAM is shown in a stick representation. Also shown in stick representation is a negatively charged MES ion. Conserved basic amino acids are labeled. (**B**) Comparison of the secondary structures of helix 31 from the small ribosomal subunit rRNAs in *S. cerevisiae* and *S. solfataricus* with the location of the hypermodified nucleotide indicated in red. For *S. solfataricus* the chemical identity of the hypermodified nucleotide is not known but the existence of *NEP1* and *TSR3* homologs suggest that it is indeed N1-methyl-N3-acp-pseudouridine. (**C**) Binding of *Ss*Tsr3 to RNA. 5′-fluoresceine labeled RNA oligonucleotides corresponding either to the native (20mer – see inset) or a stabilized (20mer_GC - inset) helix 31 of the small ribosomal subunit rRNA from *S. solfataricus* were titrated with increasing amounts of *Ss*Tsr3 and the changes in the fluoresceine fluorescence anisotropy were measured and fitted to a binding curve (20mer – red, 20mer_GC – blue). Oligo-U9-RNA was used for comparison (black). The 20mer_GC RNA was also titrated with *Ss*Tsr3 in the presence of 2 mM SAM (purple). (**D**) Mutants of *Sc*Tsr3 R60, K65 or R131 (equivalent to K17, K22 and R91 in *Vd*Tsr3) expressed in *Δtsr3* yeast cells show a primer extension stop comparable to the wild type. Combination of the three point mutations (R60A/K65A/R131A) leads to a strongly reduced acp modification of 18S rRNA.

toplasmic pre-40S particles contain 20S rRNA and at least seven non-ribosomal proteins including the D-site endonuclease Nob1 as well as Tsr1, a putative GTPase and Rio2 which block the mRNA channel and the initiator tRNA binding site, respectively, thus preventing translation initiation.

After structural changes, possibly driven by GTP hydrolysis, which go together with the formation of the decoding site, the 20S pre-rRNA becomes accessible for Nob1 cleavage at site D. This also involves joining of pre-40S and 60S subunits to 80S-like particles in a translation-like cycle promoted by eIF5B (59,60). The cleavage step most likely acts as a quality control check that ensures the proper 40S subunit assembly with only completely processed precursors (59). Finally, termination factor Rli1, an ATPase, promotes the dissociation of assembly factors and the 80S-like complex dissociates and releases the mature 40S subunit (60).

Interestingly, differences in the level of acp modification were demonstrated for different steps of the cytoplasmic pre-40S subunit maturation after analyzing purified 20S pre-rRNAs using different purification bait proteins. Early cytoplasmic pre-40S subunits still containing the ribosome assembly factors Tsr1, Ltv1, Enp1 and Rio2 were not or only partially acp modified. In contrast, late pre-40S subunits containing Nob1 and Rio1 or already associated with 60S subunits in 80S-like particles showed acp modification levels comparable to mature 40S subunits. Thus, the acp transfer to $m^1\Psi$1191 occurs during the step at which Rio2 leaves the pre-40S particle (27).

These data and the finding that a missing acp modification hinders pre-20S rRNA processing, suggest that the acp modification together with the release of Rio2 promotes the formation of the decoding site and thus D-site cleavage by Nob1. The interrelation between acp modification and Rio2 release is also supported by CRAC analysis showing that Rio2 binds to helix 31 next to the Ψ1191 residue that receives the acp modification (56). Therefore, Rio2 either blocks the access of Tsr3 to helix 31, and acp modification can only occur after Rio2 is released, or the acp modification of $m^1\Psi$1191 and putative subsequent conformational changes of 20S rRNA weaken the binding of Rio2 to helix 31 and support its release from the pre-rRNA.

In summary, by identifying Tsr3 as the enzyme responsible for introducing the acp group to the hypermodified $m^1acp^3\Psi$ nucleotide at position 1191 (yeast)/ 1248 (humans) of 18S rRNA we added one of the last remaining

pieces to the puzzle of eukaryotic small ribosomal subunit rRNA modifications. The current data together with the finding that acp modification takes place at the very last step in pre-40S subunit maturation (27) indicate that the acp modification probably supports the formation of the decoding site and efficient 20S pre-rRNA D-site cleavage. Furthermore, our structural data unravelled how the regioselectivity of SAM-dependent group transfer reactions can be tuned by distinct small evolutionary adaptions of the ligand binding pocket of SAM-binding enzymes.

ACCESSION NUMBERS

Coordinates and structure factors have been deposited in the Protein Data Bank under accession codes PDB 5APG (*Vd*Tsr3/SAM-complex) and PDB 5AP8 (*Ss*Tsr3).

SUPPLEMENTARY DATA

Supplementary Data are available at NAR Online.

ACKNOWLEDGEMENTS

The authors like to thank Peter Watzinger for excellent technical assistance and Martin Pos (Department of Biochemistry, Goethe University) for access to the crystallization facility. We acknowledge the Paul Scherrer Institute, Villigen, Switzerland, for provision of synchrotron radiation beam time at the beamlines PX and PXIII of the SLS and thank Meitian Wang and Vincent Olieric for assistance.

FUNDING

DFG grant [En134/9-1]; SFB 902 (Molecular Principles of RNA-based Regulation); DFG SPP1784 (Chemical Biology of Native Nucleic Acid Modifications, DFG grants) [En134/13-1, Wo 901/5-1]; European Community's Seventh Framework Programme [FP7/2007-2013] under BioStruct-X [283570]; Goethe University and the State of Hesse; EMBO long-term fellowship [ALTF 644-2014 to S.S.]; Research in the Lab of DLJL is supported by the Université Libre de Bruxelles (ULB); Fonds National de la Recherche (F.R.S./FNRS); Walloon Region [DGO6]; Fédération Wallonie-Bruxelles; European Research Development Fund (ERDF). Funding for open access charge: DFG SPP1784 (Chemical Biology of Native Nucleic Acid Modifications, DFG grants) [En134/13-1, Wo 901/5-1].
Conflict of interest statement. None declared.

REFERENCES

1. Woolford,J.L. Jr and Baserga,S.J. (2013) Ribosome biogenesis in the yeast Saccharomyces cerevisiae. *Genetics*, **195**, 643–681.
2. Armistead,J. and Triggs-Raine,B. (2014) Diverse diseases from a ubiquitous process: the ribosomopathy paradox. *FEBS Lett.*, **588**, 1491–1500.
3. McCann,K.L. and Baserga,S.J. (2013) Genetics. Mysterious ribosomopathies. *Science (New York, N.Y.)*, **341**, 849–850.
4. Sondalle,S.B. and Baserga,S.J. (2014) Human diseases of the SSU processome. *Biochim. Biophys. Acta*, **1842**, 758–764.
5. Kiss-Laszlo,Z., Henry,Y., Bachellerie,J.P., Caizergues-Ferrer,M. and Kiss,T. (1996) Site-specific ribose methylation of preribosomal RNA. a novel function for small nucleolar RNAs. *Cell*, **85**, 1077–1088.
6. Ganot,P., Bortolin,M.L. and Kiss,T. (1997) Site-specific pseudouridine formation in preribosomal RNA is guided by small nucleolar RNAs. *Cell*, **89**, 799–809.
7. Sharma,S. and Lafontaine,D.L.J. (2015) 'View from a bridge': a new perspective on eukaryotic rRNA base modification. *Trends Biochem. Sci.*, **40**, 560–575.
8. Peifer,C., Sharma,S., Watzinger,P., Lamberth,S., Kötter,P. and Entian,K.-D. (2013) Yeast Rrp8p, a novel methyltransferase responsible for m1A 645 base modification of 25S rRNA. *Nucleic Acids Res.*, **41**, 1151–1163.
9. Sharma,S., Yang,J., Watzinger,P., Kotter,P. and Entian,K.-D. (2013) Yeast Nop2 and Rcm1 methylate C2870 and C2278 of the 25S rRNA, respectively. *Nucleic Acids Res.*, **41**, 9062–9076.
10. Schosserer,M., Minois,N., Angerer,T.B., Amring,M., Dellago,H., Harreither,E., Calle-Perez,A., Pircher,A., Gerstl,M.P., Pfeifenberger,S. *et al.* (2015) Methylation of ribosomal RNA by NSUN5 is a conserved mechanism modulating organismal lifespan. *Nat. Commun.*, **6**, 6158.
11. Helm,M. (2006) Post-transcriptional nucleotide modification and alternative folding of RNA. *Nucleic Acids Res.*, **34**, 721–733.
12. Chow,C.S., Lamichhane,T.N. and Mahto,S.K. (2007) Expanding the nucleotide repertoire of the ribosome with post-transcriptional modifications. *ACS Chem. Biol.*, **2**, 610–619.
13. Ishitani,R., Yokoyama,S. and Nureki,O. (2008) Structure, dynamics, and function of RNA modification enzymes. *Curr. Opin. Struct. Biol.*, **18**, 330–339.
14. Decatur,W.A. and Fournier,M.J. (2002) rRNA modifications and ribosome function. *Trends Biochem. Sci.*, **27**, 344–351.
15. Baxter-Roshek,J.L., Petrov,A.N. and Dinman,J.D. (2007) Optimization of ribosome structure and function by rRNA base modification. *PLoS One*, **2**, e174.
16. Liang,X.H., Liu,Q. and Fournier,M.J. (2009) Loss of rRNA modifications in the decoding center of the ribosome impairs translation and strongly delays pre-rRNA processing. *RNA*, **15**, 1716–1728.
17. King,T.H., Liu,B., McCully,R.R. and Fournier,M.J. (2003) Ribosome structure and activity are altered in cells lacking snoRNPs that form pseudouridines in the peptidyl transferase center. *Mol. Cell*, **11**, 425–435.
18. Narla,A. and Ebert,B.L. (2010) Ribosomopathies: human disorders of ribosome dysfunction. *Blood*, **115**, 3196–3205.
19. Lafontaine,D.L.J. (2015) Noncoding RNAs in eukaryotic ribosome biogenesis and function. *Nat. Struct. Mol. Biol.*, **22**, 11–19.
20. Sato,G., Saijo,Y., Uchiyama,B., Kumano,N., Sugawara,S., Fujimura,S., Sato,M., Sagawa,M., Ohkuda,K., Koike,K. *et al.* (1999) Prognostic value of nucleolar protein p120 in patients with resected lung adenocarcinoma. *J. Clin. Oncol.*, **17**, 2721–2727.
21. Enger,M.D. and Saponara,A.G. (1968) Incorporation of 14C from [2-14C]methionine into 18 s but not 28 s RNA of Chinese hamster cells. *J. Mol. Biol.*, **33**, 319–322.
22. Samarsky,D.A., Balakin,A.G. and Fournier,M.J. (1995) Characterization of three new snRNAs from Saccharomyces cerevisiae. snR34, snR35 and snR36. *Nucleic Acids Res.*, **23**, 2548–2554.
23. Taylor,A.B., Meyer,B., Leal,B.Z., Kötter,P., Schirf,V., Demeler,B., Hart,P.J., Entian,K.-D. and Wöhnert,J. (2008) The crystal structure of Nep1 reveals an extended SPOUT-class methyltransferase fold and a pre-organized SAM-binding site. *Nucleic Acids Res.*, **36**, 1542–1554.
24. Wurm,J.P., Meyer,B., Bahr,U., Held,M., Frolow,O., Kotter,P., Engels,J.W., Heckel,A., Karas,M., Entian,K.D. *et al.* (2010) The ribosome assembly factor Nep1 responsible for Bowen-Conradi syndrome is a pseudouridine-N1-specific methyltransferase. *Nucleic Acids Res.*, **38**, 2387–2398.
25. Meyer,B., Wurm,J.P., Kötter,P., Leisegang,M.S., Schilling,V., Buchhaupt,M., Held,M., Bahr,U., Karas,M., Heckel,A. *et al.* (2011) The Bowen-Conradi syndrome protein Nep1 (Emg1) has a dual role in eukaryotic ribosome biogenesis, as an essential assembly factor and in the methylation of Ψ1191 in yeast 18S rRNA. *Nucleic Acids Res.*, **39**, 1526–1537.
26. Brand,R.C., Klootwijk,J., Planta,R.J. and Maden,B.E. (1978) Biosynthesis of a hypermodified nucleotide in Saccharomyces carlsbergensis 17S and HeLa-cell 18S ribosomal ribonucleic acid. *Biochem J.*, **169**, 71–77.

27. Hector,R.D., Burlacu,E., Aitken,S., Le Bihan,T., Tuijtel,M., Zaplatina,A., Cook,A.G. and Granneman,S. (2014) Snapshots of pre-rRNA structural flexibility reveal eukaryotic 40S assembly dynamics at nucleotide resolution. *Nucleic Acids Res.*, **42**, 12138–12154.
28. Lin,H. (2011) S-Adenosylmethionine-dependent alkylation reactions: when are radical reactions used? *Bioorg. Chem.*, **39**, 161–170.
29. Noma,A., Kirino,Y., Ikeuchi,Y. and Suzuki,T. (2006) Biosynthesis of wybutosine, a hyper-modified nucleoside in eukaryotic phenylalanine tRNA. *EMBO J.*, **25**, 2142–2154.
30. Umitsu,M., Nishimasu,H., Noma,A., Suzuki,T., Ishitani,R. and Nureki,O. (2009) Structural basis of AdoMet-dependent aminocarboxypropyl transfer reaction catalyzed by tRNA-wybutosine synthesizing enzyme, TYW2. *Proc. Natl. Acad. Sci. U.S.A.*, **106**, 15616–15621.
31. Schaffrath,R., Abdel-Fattah Mohamed,W., Klassen,R. and Stark,M.J. (2014) The diphthamide modification pathway from Saccharomyces cerevisiae - revisited. *Mol. Microbiol.*, **94**, 1213–1226.
32. Mattheakis,L.C., Sor,F. and Collier,R.J. (1993) Diphthamide synthesis in Saccharomyces cerevisiae: structure of the DPH2 gene. *Gene*, **132**, 149–154.
33. Liu,S., Milne,G.T., Kuremsky,J.G., Fink,G.R. and Leppla,S.H. (2004) Identification of the proteins required for biosynthesis of diphthamide, the target of bacterial ADP-ribosylating toxins on translation elongation factor 2. *Mol. Cell. Biol.*, **24**, 9487–9497.
34. Li,Z., Lee,I., Moradi,E., Hung,N.-J., Johnson,A.W. and Marcotte,E.M. (2009) Rational extension of the ribosome biogenesis pathway using network-guided genetics. *PLoS Biol.*, **7**, e1000213.
35. Burroughs,A.M. and Aravind,L. (2014) Analysis of two domains with novel RNA-processing activities throws light on the complex evolution of ribosomal RNA biogenesis. *Front. Genet.*, **5**, 424.
36. Gehrke,C.W. and Kuo,K.C. (1989) Ribonucleoside analysis by reversed-phase high-performance liquid chromatography. *J. Chromatogr.*, **471**, 3–36.
37. Sambrook,J. and Russell,D. (2001) *Molecular Cloning. A Laboratory Manual*. Cold Spring Harbor Laboratory Press, NY.
38. Sharma,S., Langhendries,J.-L., Watzinger,P., Kotter,P., Entian,K.-D. and Lafontaine,D.L.J. (2015) Yeast Kre33 and human NAT10 are conserved 18S rRNA cytosine acetyltransferases that modify tRNAs assisted by the adaptor Tan1/THUMPD1. *Nucleic Acids Res.*, **43**, 2242–2258.
39. Sharma,S., Yang,J., Düttmann,S., Watzinger,P., Kötter,P. and Entian,K.-D. (2014) Identification of novel methyltransferases, Bmt5 and Bmt6, responsible for the m3U methylations of 25S rRNA in Saccharomyces cerevisiae. *Nucleic Acids Res.*, **42**, 3246–3260.
40. Huh,W.K., Falvo,J.V., Gerke,L.C., Carroll,A.S., Howson,R.W., Weissman,J.S. and O'Shea,E.K. (2003) Global analysis of protein localization in budding yeast. *Nature*, **425**, 686–691.
41. Maden,B.E., Forbes,J., de Jonge,P. and Klootwijk,J. (1975) Presence of a hypermodified nucleotide in HeLa cell 18 S and Saccharomyces carlsbergensis 17 S ribosomal RNAs. *FEBS Lett.*, **59**, 60–63.
42. Buchhaupt,M., Kötter,P. and Entian,K.D. (2007) Mutations in the nucleolar proteins Tma23 and Nop6 suppress the malfunction of the Nep1 protein. *FEMS Yeast Res.*, **7**, 771–781.
43. Eschrich,D., Buchhaupt,M., Kötter,P. and Entian,K.D. (2002) Nep1p (Emg1p), a novel protein conserved in eukaryotes and archaea, is involved in ribosome biogenesis. *Curr. Genet.*, **40**, 326–338.
44. Armengaud,J., Dedieu,A., Solques,O., Pellequer,J.-L. and Quemeneur,E. (2005) Deciphering structure and topology of conserved COG2042 orphan proteins. *BMC Struct. Biol.*, **5**, 3.
45. Woese,C.R., Gupta,R., Hahn,C.M., Zillig,W. and Tu,J. (1984) The phylogenetic relationships of three sulfur dependent archaebacteria. *Syst. Appl. Microbiol.*, **5**, 97–105.
46. Karcher,A., Schele,A. and Hopfner,K.-P. (2008) X-ray structure of the complete ABC enzyme ABCE1 from Pyrococcus abyssi. *J. Biol. Chem.*, **283**, 7962–7971.
47. Jackman,J.E., Montange,R.K., Malik,H.S. and Phizicky,E.M. (2003) Identification of the yeast gene encoding the tRNA m1G methyltransferase responsible for modification at position 9. *RNA*, **9**, 574–585.
48. Shao,Z., Yan,W., Peng,J., Zuo,X., Zou,Y., Li,F., Gong,D., Ma,R., Wu,J., Shi,Y. *et al.* (2014) Crystal structure of tRNA m1G9 methyltransferase Trm10: insight into the catalytic mechanism and recognition of tRNA substrate. *Nucleic Acids Res.*, **42**, 509–525.
49. Ben-Shem,A., Jenner,L., Yusupova,G. and Yusupov,M. (2010) Crystal structure of the eukaryotic ribosome. *Science (New York, N.Y.)*, **330**, 1203–1209.
50. Kowalak,J.A., Bruenger,E., Crain,P.F. and McCloskey,J.A. (2000) Identities and phylogenetic comparisons of posttranscriptional modifications in 16 S ribosomal RNA from Haloferax volcanii. *J. Biol. Chem.*, **275**, 24484–24489.
51. Jones,W., Leigh,J., Mayer,F., Woese,C.R. and Wolfe,R. (1983) Methanococcus jannaschii sp. nov., an extremely thermophilic methanogen from a submarine hydrothermal vent. *Arch. Microbiol.*, **136**, 254–261.
52. Lafontaine,D., Delcour,J., Glasser,A.L., Desgres,J. and Vandenhaute,J. (1994) The DIM1 gene responsible for the conserved m6(2)Am6(2)A dimethylation in the 3'-terminal loop of 18 S rRNA is essential in yeast. *J. Mol. Biol.*, **241**, 492–497.
53. White,J., Li,Z., Sardana,R., Bujnicki,J.M., Marcotte,E.M. and Johnson,A.W. (2008) Bud23 methylates G1575 of 18S rRNA and is required for efficient nuclear export of pre-40S subunits. *Mol. Cell. Biol.*, **28**, 3151–3161.
54. Zorbas,C., Nicolas,E., Wacheul,L., Huvelle,E., Heurgué-Hamard,V. and Lafontaine,D.L.J. (2015) The human 18S rRNA base methyltransferases DIMT1L and WBSCR22-TRMT112 but not rRNA modification are required for ribosome biogenesis. *Mol. Biol. Cell*, **26**, 2080–2095.
55. Leulliot,N., Bohnsack,M.T., Graille,M., Tollervey,D. and van Tilbeurgh,H. (2008) The yeast ribosome synthesis factor Emg1 is a novel member of the superfamily of alpha/beta knot fold methyltransferases. *Nucleic Acids Res.*, **36**, 629–639.
56. Granneman,S., Petfalski,E., Swiatkowska,A. and Tollervey,D. (2010) Cracking pre-40S ribosomal subunit structure by systematic analyses of RNA-protein cross-linking. *EMBO J.*, **29**, 2026–2036.
57. Strunk,B.S., Loucks,C.R., Su,M., Vashisth,H., Cheng,S., Schilling,J., Brooks,C.L., Karbstein,K. and Skiniotis,G. (2011) Ribosome assembly factors prevent premature translation initiation by 40S assembly intermediates. *Science (New York, N.Y.)*, **333**, 1449–1453.
58. Hellmich,U.A., Weis,B.L., Lioutikov,A., Wurm,J.P., Kaiser,M., Christ,N.A., Hantke,K., Kötter,P., Entian,K.-D., Schleiff,E. *et al.* (2013) Essential ribosome assembly factor Fap7 regulates a hierarchy of RNA-protein interactions during small ribosomal subunit biogenesis. *Proc. Natl. Acad. Sci. U.S.A.*, **110**, 15253–15258.
59. Lebaron,S., Schneider,C., van Nues,R.W., Swiatkowska,A., Walsh,D., Böttcher,B., Granneman,S., Watkins,N.J. and Tollervey,D. (2012) Proofreading of pre-40S ribosome maturation by a translation initiation factor and 60S subunits. *Nat. Struct. Mol. Biol.*, **19**, 744–753.
60. Strunk,B.S., Novak,M.N., Young,C.L. and Karbstein,K. (2012) A translation-like cycle is a quality control checkpoint for maturing 40S ribosome subunits. *Cell*, **150**, 111–121.